Chinese Physics B

PAPER

Enhancement of isolated attosecond pulse generation by using long gas medium

Enhancement of isolated attosecond pulse generation by using long gas medium

Yueying Liang(梁玥瑛)[1,3], Xinkui He(贺新奎)[1,2,3,†], Kun Zhao(赵昆)[1], Hao Teng(滕浩)[1], and Zhiyi Wei(魏志义)[1,2,3,‡]

[1] *Beijing National Laboratory for Condensed Matter Physics, Institute of Physics, Chinese Academy of Sciences, Beijing* 100190, *China*
[2] *Songshan Lake Materials Laboratory, Dongguan* 523808, *China*
[3] *University of Chinese Academy of Sciences, Beijing* 100049, *China*

(Received 16 June 2021; revised manuscript received 13 September 2021; accepted manuscript online 24 September 2021)

Isolated attosecond pulse generation in argon is theoretically investigated for different gas pressures and medium lengths. The output of attosecond pulse is effectively enhanced by using a longer gas medium with optimized pressure. The peak intensity of the attosecond pulse by using 6 mm gas medium is doubled compared with that of 1–3 mm gas cell, which is usually used in the experiment. Our simulation shows that the distortion of the driving laser waveform and the absorption are the main factors that limit the output of the attosecond pulse for the long gas medium. Optimized generation condition could be found by balancing the medium length and pressure.

Keywords: isolated attosecond pulse, high-order harmonic generation

PACS: 33.20.Xx **DOI:** 10.1088/1674-1056/ac29a8

1. Introduction

The development of attosecond physics, especially the generation of isolated attosecond pulse (IAP), provides unprecedented approaches for studying ultrafast phenomena in attosecond time scale. In the last two decades, isolated attosecond pulses are widely used in the attosecond time-resolved detection of the ultrafast process with different methods such as attosecond streaking[1] and attosecond transient absorption.[2] Currently, IAP is obtained from the high-order harmonic generation (HHG) process,[3] which produces broadband coherent radiation in extreme ultraviolet (XUV) range. Temporally this radiation consists of attosecond pulses with a separation of half-cycle of fundamental laser. IAP can be selected from the attosecond pulse train by using gating methods including amplitude gating,[1] polarization gating,[4] ionization gating[5] as well as attosecond lighthouse.[6] As an extreme-high order nonlinear optical effect, the efficiency of HHG is lower than 10^{-6}[7,8] in general, decreasing with the increase of photon energy and the driving laser wavelength.[9] Since the gating methods for IAP selection normally demand a few-cycle driving pulse with stabilized carrier envelope phase (CEP), it has become a significant work to develop such kind of driving laser with high pulse energy. However, up to now, the available lasers with controlled CEP and enough short pulse duration are mainly limited with pulse energy less than 1 mJ.[10] With the limitation of the low driving pulse energy and the low conversion efficiency, the energy of IAP is normally only in the pJ to nJ level,[8] which severely restricts its applications. For example, the characterization of attosecond pulse is mostly done by attosecond streaking camera, which is a cross-correlation measurement between the fundamental laser pulse and the IAP.[1] The autocorrelation measurement of attosecond pulse with high temporal resolution is still very difficult to be carried out due to the extremely low energy of IAP.[11–13] To overcome this difficulty, improvement of the output pulse energy has become one of the most important issues for attosecond physics.

Optimization of the conversion efficiency of HHG has been well investigated both theoretically and experimentally, considering the single atom response and the macroscopic effect. Single atom response can be improved by using two-color or multi-color laser field. The breaking up of half-cycle symmetry of the attosecond generation not only increases the efficiency, but also relax the restrictions of the pulse duration of driving lasers.[14] As the harmonics detected at the exit of the gas cell is the coherent sum of the harmonics generated by every single atom along the gas cell, the total energy of the harmonics reaches maximum only when the single atom responses are phase matched. By adjusting the gas pressure,[15] the position of gas cell relative to the laser focus and the length of gas cell, the phase matching condition can be optimized to enhance the conversion efficiency of HHG.[16] Therefore, the optimized length of gas medium for a certain order of harmonic is closely related to the species of gas, the pressure and the focusing scheme which influences the phase matching condition.[17] Most of the work on phase-matching optimization uses long driving pulse and focuses on the total output or certain order of the harmonics. However for IAP generation,

†Corresponding author. E-mail: xinkuihe@iphy.ac.cn
‡Corresponding author. E-mail: zywei@iphy.ac.cn

the phase matching condition should be optimized in a wide spectral range, and most importantly the phase synchronization of the radiation in that spectral range need to be checked. Because of the experimental complexity, it is difficult to optimize the gas cell length continuously in real time. In experiments for IAP generation, the length of gas cell is normally set to be 1–3 mm.[1,18] In this paper, the optimized condition of gas medium and the group delay dispersion (GDD) of the generated pulse is theoretically explored. The result shows that the intensity of IAP can be effectively enhanced while keeping the short pulse duration by using longer gas medium. Our simulation gives a reference for experiments in generating IAP with high-flux and short pulse duration at the same time.

2. Theoretical model

To obtain the intensity of the IAP at the exit of the gas medium,[19] we calculated the single-atom response using the strong-field approximation (SFA),[19,20] combined with the coupled 3D Maxwell's wave equations describing the propagation effect. The nonlinear dipole moment in the time domain (in atomic units) is expressed as

$$d_{\mathrm{nl}}(t) = 2\mathrm{Re}\left\{\mathrm{i}\int_{-\infty}^{t}\mathrm{d}t'\left(\frac{\pi}{\varepsilon+\mathrm{i}(t-t')/2}\right)^{3/2}\right.$$
$$\times d^{*}\left[p_{\mathrm{st}}(t',t)-A(t)\right]d\left[p_{\mathrm{st}}(t',t)-A(t')\right]$$
$$\left.\times\exp\left[-\mathrm{i}S_{\mathrm{st}}(t',t)\right]E_{\mathrm{l}}(t')\right\}a(t), \tag{1}$$

where $E_{\mathrm{l}}(t)$ is the electric field of the driving laser, $A(t)$ is the corresponding vector potential, and ε is a positive regularization constant. p_{st} and S_{st} are the canonical momentum and quasiclassical action at the stationary point.[19] The dipole matrix element from the ground state to a continuum state for hydrogen-like atoms is approximated as

$$d(p) = \mathrm{i}\frac{2^{7/2}(2I_{\mathrm{p}})^{5/4}}{\pi}\frac{p}{(p^2+2I_{\mathrm{p}})^3}, \tag{2}$$

where I_{p} is the ionization potential of the atom. The ground state amplitude is calculated by

$$a(t) = \exp\left[-\int_{-\infty}^{t}w(t')\,\mathrm{d}t'\right], \tag{3}$$

where $w(t')$ is the tunnel ionization rate in the Ammosov–Delone–Krainov (ADK) theory.

By using the paraxial approximation in a moving frame ($z'=z$ and $t'=t-z/c$), in the frequency domain, the propagation process of the driving laser and high harmonic fields can be described by the following equations:

$$\nabla_{\perp}^2\widetilde{E}_{\mathrm{l}}(r,z',\omega) - \frac{2\mathrm{i}\omega}{c}\frac{\partial\widetilde{E}_{\mathrm{l}}(r,z',\omega)}{\partial z'} = \widetilde{G}_{\mathrm{l}}(r,z',\omega), \tag{4}$$

$$\nabla_{\perp}^2\widetilde{E_{\mathrm{h}}}(r,z',\omega) - \frac{2\mathrm{i}\omega}{c}\left(\frac{\partial\widetilde{E_{\mathrm{h}}}(r,z',\omega)}{\partial z'} + \frac{\alpha(\omega)}{2}\widetilde{E_{\mathrm{h}}}(r,z',\omega)\right) = \widetilde{G_{\mathrm{h}}}(r,z',\omega), \tag{5}$$

where $\widetilde{E}_{\mathrm{l}}$ and $\widetilde{E_{\mathrm{h}}}$ are the Fourier transforms of the laser field $E_{\mathrm{l}}(r,z',t')$ and harmonic field $E_{\mathrm{h}}(r,z',t')$, respectively, and α is the XUV absorption coefficient. The source term of the fundamental laser is calculated by

$$\widetilde{G}_{\mathrm{l}}(r,z',\omega) = \widehat{F}\left(\frac{\omega_{\mathrm{p}}^2(r,z',t')}{c^2}E_{\mathrm{l}}(r,z',t')\right), \tag{6}$$

where $\widehat{F}$ is the Fourier transform operator,

$$\omega_{\mathrm{p}}(r,z,t) = \left(\frac{e^2n_{\mathrm{e}}(r,z,t)}{\varepsilon_0 m_{\mathrm{e}}}\right)^{1/2} \tag{7}$$

is the plasma frequency, e, n_{e} and m_{e} are the electron charge, free-electron density and electron mass, respectively. For the high order harmonics,

$$\widetilde{G_{\mathrm{h}}}(r,z',\omega) = \hat{F}\left[\frac{\omega_{\mathrm{p}}(r,z',t')^2}{c^2}E_{\mathrm{h}}(r,z',t') + \mu_0\frac{\partial^2P_{\mathrm{nl}}(r,z',t')}{\partial t^2}\right], \tag{8}$$

and $P_{\mathrm{nl}}(r,z,t) = [n_0 - n_{\mathrm{e}}(r,z,t)]d_{\mathrm{nl}}(r,z,t)$ is the nonlinear polarization. The ionization effect and the absorption of the HHG are included in the calculation,[21] as they could affect the peak intensity of the fundamental laser and attosecond pulse at long propagation length and high gas pressure.

The total intensity of attosecond pulses is calculated by integrating the intensity over the whole cross section at the exit position z_{out} of gas medium

$$I_{\mathrm{h}}(t) \propto \int_0^{\infty}|E_{\mathrm{h}}(r,z_{\mathrm{out}},t)|^2 2\pi r\,\mathrm{d}r. \tag{9}$$

3. Results and discussion

In our simulation, the driving laser is assumed to be Gaussian in both the temporal domain and spatial domain, with the pulse duration of 5 fs at the central wavelength of 800 nm. The peak intensity at the laser focus is 3×10^{14} W/cm^2. The beam waist is set to be 50 μm, with the Rayleigh length about 10 mm. The center of the gas medium filled with argon is positioned at the laser focus so that the laser intensity keeps above 10^{14} W/cm^2 in the whole range of gas target. Amplitude gating is used in order to obtain an IAP with the selected

continuum spectrum higher than 54 eV at the cutoff region. The parameters used in our simulation are chosen to be close to the common experimental conditions, therefore the results in this paper could be taken as a good reference for the experiments.

The peak intensity of the selected IAP as a function of the gas medium length at the gas pressure from 20 Torr to 50 Torr is shown in Fig. 1. For all the gas pressures, when the medium length is shorter than 0.5 mm, the peak intensity of IAP is proportional to the gas pressure approximately, and it is quiet small compared to the maximum peak intensity. In this case, the gas medium is short enough to be regarded as a thin layer, and the intensity of IAP is mostly dominated by the single atom response. The phase matching effect and the absorption effect have almost no contribution to the total intensity of IAP. The phase matching effect is more significant when the length of the gas medium becomes longer. For low gas pressure at 20 Torr, the peak intensity of IAP saturates at 4 mm gas medium, then keeps almost unchanged with the increase of the gas medium length. At high gas pressure, for example at 50 Torr, the optimized gas medium is 2 mm, shorter than that of the low gas pressure. Then the peak intensity of IAP rapidly decrease with the increasing gas medium length, showing the bad phase-matching and strong absorption. For the optimized gas pressure of 30 Torr, the peak intensity of IAP gradually increases with the increase of the length of the gas medium, and reaches a maximum at 6 mm gas medium. Compared with the IAP generated by 1 mm gas medium, the peak intensity of the IAP by using 6 mm gas medium at the gas pressure of 30 Torr is enhanced by about an order of magnitude. The results indicate that it is efficient to improve the peak intensity of IAP by optimizing the phase matching condition with proper gas pressure and gas medium length.

To understand the phase matching process of IAP during the generation and propagation, the time-frequency analysis[22] of attosecond bursts at the gas pressure of 30 Torr and 50 Torr is shown in Fig. 2. In the case of 1 mm gas medium, for the continuum spectrum above 54 eV, the difference of the time-frequency analysis between 30 Torr and 50 Torr is quite small. As the gas medium increases to 3 mm, the enhanced part of the spectrum around $t = 0$ is mainly from 39 eV to 67 eV at 30 Torr in Fig. 2(b), compared to that from 34 eV to 59 eV at 50 Torr in Fig. 2(f). In other word, the phase-matching for spectrum in the cutoff region is getting worse with an increase of the gas pressure. Furthermore, the difference of the cutoff frequency of the attosecond bursts around $t = 0$ and $t = 0.5$ optical cycle (o.c.) is quite small, which reduces the temporal contrast of the selected IAP. As the gas target extends to 6 mm, the intensity of the cutoff region keeps increasing at 30 Torr, leading to the enhancement of the IAP. In the case of 50 Torr, the intensity of the whole spectrum decreases, and the long trajectory begins to appear. The cutoff frequency decreases both at 30 Torr and 50 Torr with the 9 mm gas medium.

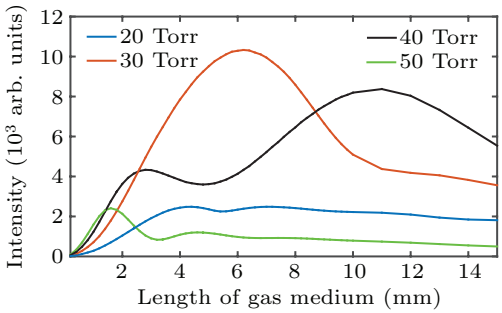

Fig. 1. The peak intensity of IAP at the exit of gas medium as a function of medium length for different gas pressure from 20 Torr to 50 Torr.

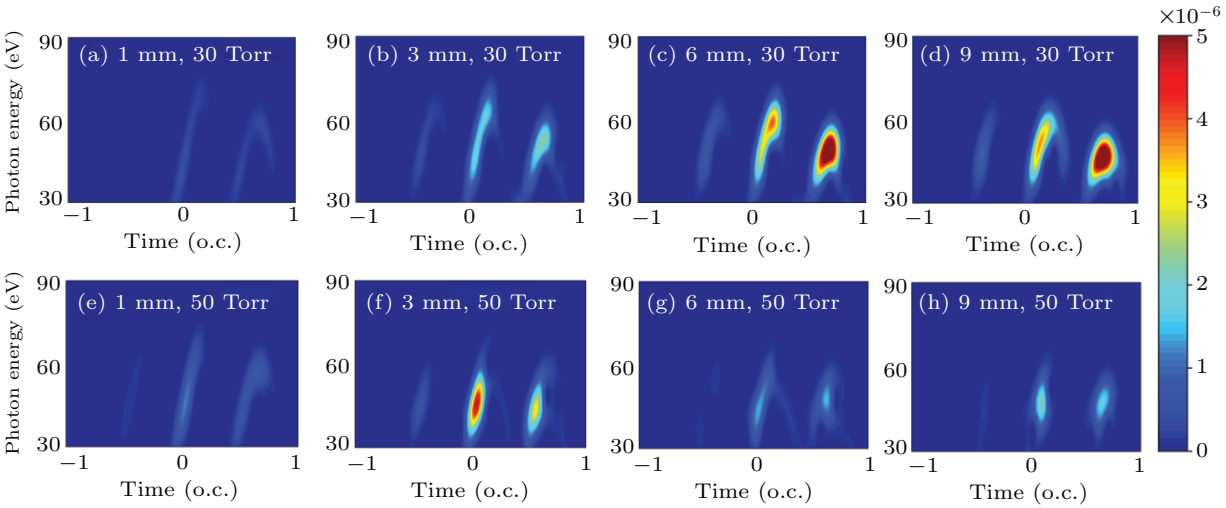

Fig. 2. On-axis time-frequency analysis of attosecond emission at the exit of gas target with medium length of (a) 1 mm, (b) 3 mm, (c) 6 mm, (d) 9 mm at the pressure of 30 Torr, and (e)–(f) with the same medium length at the pressure of 50 Torr.

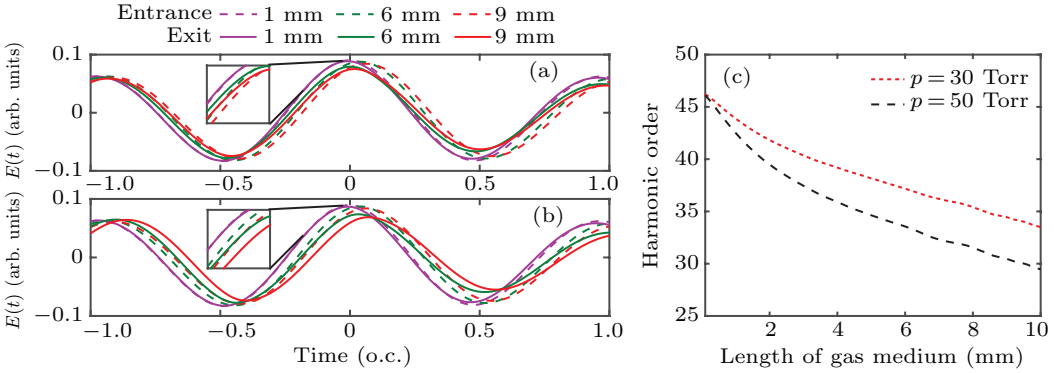

Fig. 3. The electric field waveform at the entrance (dashed line) and the exit (solid line) of gas medium with length of 1 mm, 6 mm, 9 mm and pressure of (a) 30 Torr, (b) 50 Torr. (c) The calculated cut-off order corresponding to the peak intensity of the driving laser.

The wave vector mismatch between the driving laser and the HHG can be written as[10,23] $\Delta k_q = \Delta k_n + \Delta k_p + \Delta k_g + \Delta k_d$. The first term stands for the neutral atom dispersion, which comes from the difference between the refractive index of the fundamental laser and the q^{th} harmonic. The second term is the contribution of the free-electron dispersion. The third term is the geometric dispersion for free space propagation. The last term is the wave vector mismatch of the dipole phase, which is related to the intensity of the driving laser and the order of harmonics.

The increase of gas pressure not only affects the number of the interaction atoms, but also influences the dispersion terms in the phase-matching equation. The laser could interact with more atoms in a certain volume at high gas pressure. As a result, the intensity of the generated high harmonics and IAP pulses is enhanced with the gas pressure when the gas medium is short, which means phase-matching condition is satisfied in this case. On the other hand, the number of the ionized electrons also increases with the gas pressure, thus enhances the plasma effect. The dispersion caused by the free electron leads to the phase mismatch, which is hard to be compensated by other terms. Therefore, the gas pressure should be well optimized to balance these two factors.

The free-electron dispersion also leads to the reshaping[24] of the fundamental field at high gas pressure and long propagation distance. In Fig. 3 we show the waveform of the driving laser at the entrance and the exit of the gas medium for gas pressure at 30 Torr and 50 Torr. For each gas pressure, the phase shift increases with the length of gas medium. For the same gas medium, compared to 50 Torr, the phase shift of the electric field is smaller at 30 Torr, especially around the peak of the laser field at $t = 0$. The significant change of the phase makes considerable phase mismatch at cutoff region, leading to short coherent length at high gas pressure, which is consistent with the result observed in the time-frequency analysis.

The peak intensity of the fundamental field drops quickly at high gas pressure due to the defocusing effect caused by the plasma,[25] which will directly decrease the highest photon energy of the attosecond pulse. The cut-off frequency calculated by $\hbar\omega_{max} = I_p + 3.17U_p = I_p + 3.17\frac{eE_0^2}{4m\omega^2}$,[26] where I_p is the atomic ionization potential, and U_p is the ponderomotive energy, at the exit of the gas medium as a function of the medium length is shown in Fig. 3(c). For example, with the gas pressure of 30 Torr and 6 mm gas medium, the cutoff order is above 37^{th}. As the gas pressure increases to 50 Torr, the cutoff order decreases to lower than 35^{th}. This indicates that harmonics with high photon energy is hard to be generated by long gas medium at high gas pressure. The dispersion of the fundamental field also reduces the difference of peak intensities between the neighboring half cycles. The change of waveform not only causes more ionized electrons before the half cycle with maximum intensity around $t = 0$, but also reduces the difference of the highest photon energy of the neighboring half cycles, making it difficult to select a continuum spectrum by using amplitude gating. In conclusion, the high free electron density at high gas pressure leads to the defocusing and dispersion of the driving laser waveform, further results in the phase mismatch as well as the narrowing of the continuum spectrum at the cutoff frequency in a long propagation distance.

The absorption of generation medium is another factor limiting the intensity of generated IAP. The absorption length, defined as the distance over which the intensity of harmonics decreases to 1/e of its initial value,[21] changes with the gas density and the photon energy. When the length of gas medium is comparable to the absorption length, the absorption effect can not be neglected. Table 1 shows the corresponding absorption length at 30 Torr and 50 Torr for the different photon energies in the cutoff region. The absorption length decreases with the photon energy and gas pressure. At the gas pressure of 50 Torr, the absorption length is only half of that at 30 Torr for the same photon energy. Thus, for the gas medium longer than 7 mm, the generated attosecond pulse at the entrance is strongly absorbed before arriving at the exit, decreasing the efficiency of IAP generation. Furthermore, the absorption of harmonics in Ar increases with the photon energy at the range from 50 eV to 70 eV, close to the calculated cutoff region. As a result, the intensity of high harmonics with high

photon energy decreases faster than the low-energy part along the gas medium at higher pressure. The strong absorption of the high-energy photons further suppresses the radiation over the continuum range at high gas pressure.

Table 1. The absorption length at the cutoff photon energy.

Photon energy (eV)		54.25	60.45	69.75
Absorption length (mm)	$P = 30$ Torr	11.2	9.3	7.5
	$P = 50$ Torr	6.7	5.6	4.5

The full width at half maximum (FWHM) pulse duration is shown in Fig. 4. The GDD in the cut-off region at 30 Torr is shown in Fig. 5, which is directly related to the shape and the duration of the attosecond pulse in time domain.[27] For example, at 30 Torr gas pressure, the GDD of the attosecond pulse generated by 2 mm gas medium is close to zero from 62 eV to 87 eV. The fluctuation of GDD from 55 eV to 62 eV is caused by the interference between the attosecond pulses generated in the neighboring half cycles,[28] which means it is not a clean IAP in that spectral range. In this case, there are two neighboring pulses generated before and after the main attosecond pulse. In the temporal domain, the amplitude of the prepulse is about 14% of the main pulse, and the amplitude of the postpulse is about 28%. In order to optimize the amplitude ratio of the main pulse to the neighboring pulses to more than 10:1, the selected spectral range should be decreased from 58 eV to 87 eV, corresponding to the pulse duration of 277 as with 85% of the original amplitude. The attosecond pulse with the minimum pulse duration is generated in 4 mm gas medium at 30 Torr. Compared to the case of 2 mm medium, the range of the continuum spectrum with GDD closed to zero expands from 59 eV to 84 eV. The amplitude ratio of the main pulse and the neighboring pulses is about 9:1, which is acceptable for the applications of IAP.

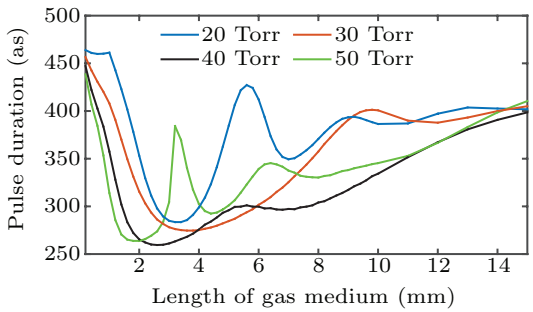

Fig. 4. The pulse duration at the exit of gas medium for different gas pressure from 20 Torr to 50 Torr. Other parameters are same as those in Fig. 1.

The extension of the continuum region benefits the generation of shorter attosecond pulse. For 6 mm gas medium, although the pulse duration increases a little due to the decrease of the cut-off frequency, the fluctuation of GDD is less than 3 fs^2 in the whole spectrum from 55 eV to 84 eV, which means that the attosecond pulse is well compressed and the pulse duration is close to the Fourier transform limit. In the case of 8 mm gas cell, the interference between the attosecond pulses leads to the strong modulation of spectral phase, making it difficult to generate IAP. The FWHM of the IAP generated at 30 Torr using 6 mm gas medium is 298.5 as, which is close to the minimum one of 271.5 as.

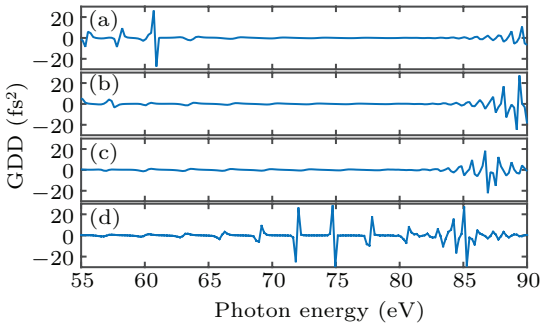

Fig. 5. The group delay dispersion on axis at the cut-off region at the gas pressure of 30 Torr generated by (a) 2 mm, (b) 4 mm, (c) 6 mm, (d) 8 mm gas medium.

4. Conclusion and perspectives

In conclusion, we theoretically investigate the phase-matching effect of IAP generation in argon. The maximum peak intensity is achieved by using 6 mm gas medium at the gas pressure of 30 Torr, which is more than doubled comparing with the case of 1–3 mm gas medium usually used in the experiment. Using the time-frequency analysis, we show that better phase-matching condition can be fulfilled by combining the optimized gas pressure and medium length, especially in the cutoff region. The corresponding pulse duration for the optimized phase-matching condition is also calculated, which is slightly longer than the minimum case. Our simulation proves that it is efficient to enhance the IAP intensity by using longer gas medium with optimized pressure. As real experimental parameters were used in the calculations, our simulation result provides a useful guidance for future experiments.

Acknowledgements

Project supported by the National Key R&D Program of China (Grant No. 2018YFB1107200) and the National Natural Science Foundation of China (Grant Nos. 11974416 and 91850209).

References

[1] Hentschel M, Kienberger R, Spielmann C, Reider G A, Milosevic N, Brabec T, Corkum P, Heinzmann U, Drescher M and Krausz F 2001 *Nature* **414** 509

[2] Holler M, Schapper F, Gallmann L and Keller U 2011 *Phys. Rev. Lett.* **106** 123601

[3] Paul P M, Toma E S, Breger P, Mullot G, Augé F, Balcou P, Muller H G and Agostini P 2001 *Science* **292** 1689

[4] Sola I, Mével E, Elouga L, Constant E, Strelkov V, Poletto L, Villoresi P, Benedetti E, Caumes J P and Stagira S 2006 *Nat. Phys.* **2** 319

[5] Abel M J, Pfeifer T, Nagel P M, Boutu W, Bell M J, Steiner C P, Neumark D M and Leone S R 2009 *Chem. Phys.* **366** 9

[6] Vincenti H and Quéré F 2012 *Phys. Rev. Lett* **108** 113904

[7] Chini M, Zhao K and Chang Z 2014 *Nat. Photon.* **8** 178

[8] Sansone G, Poletto L and Nisoli M 2011 *Nat. Photon.* **5** 655

[9] Shiner A, Trallero-Herrero C, Kajumba N, Bandulet H C, Comtois D, LégaréF, Giguère M, Kieffer J, Corkum P and Villeneuve D 2009 *Phys. Rev. Lett.* **103** 073902

[10] Heyl C, Arnold C, Couairon A and L'Huillier A 2016 *J. Phys. B: Atom. Mol. Opt. Phys.* **50** 013001

[11] Eckle P, Smolarski M, Schlup P, Biegert J, Staudte A, Schöffler M, Muller H G, Dörner R and Keller U 2008 *Nat. Phys.* **4** 565

[12] Tzallas P, Charalambidis D, Papadogiannis N, Witte K and Tsakiris G D 2003 *Nature* **426** 267

[13] Nabekawa Y, Shimizu T, Okino T, Furusawa K, Hasegawa H, Yamanouchi K and Midorikawa K 2006 *Phys. Rev. Lett* **96** 083901

[14] Chang 2007 *Phys. Rev. A* **76** 051403

[15] Wang G, Jin C, Le A T and Lin C 2011 *Phys. Rev. A* **84** 053404

[16] Rothhardt J, Krebs M, Hädrich S, Demmler S, Limpert J and Tünnermann A 2014 *New J. Phys.* **16** 033022

[17] Delfin C, Altucci C, De Filippo F, De Lisio C, Gaarde M, L'Huillier A, Roos L and Wahlström 1999 *J. Phys. B: Atom. Mol. Opt. Phys.* **32** 5397

[18] Li J, Ren X, Yin Y, Zhao K, Chew A, Cheng Y, Cunningham E, Wang Y, Hu S and Wu Y 2017 *Nat. Commun.* **8** 1

[19] Priori E, Cerullo G, Nisoli M, Stagira S, De Silvestri S, Villoresi P, Poletto L, Ceccherini P, Altucci C and Bruzzese R 2000 *Phys. Rev. A* **61** 063801

[20] Lewenstein M, Balcou P, Ivanov M Y, L'huillier A and Corkum P B 1994 *Phys. Rev. A* **49** 2117

[21] Constant E, Garzella D, Breger P, Mével E, Dorrer C, Le Blanc C, Salin F and Agostini P 1999 *Phys. Rev. Lett.* **82** 1668

[22] Yakovlev V S and Scrinzi A 2003 *Phys. Rev. Lett.* **91** 153901

[23] Pfeifer T, Spielmann C and Gerber G 2006 *Rep. Prog. Phys.* **69** 443

[24] Jin C and Lin C D 2016 *Phys. Rev. A* **94** 043804

[25] Bellini M, Corsi C and Gambino M 2001 *Phys. Rev. A* **64** 023411

[26] Chang Z 2016 *Fundamentals of Attosecond Optics* p. 171

[27] Agrawal G P 2000 *Nonlinear Fib. Opt.* p. 195

[28] Varjú K, Mairesse Y, Carré B, Gaarde M B, Johnsson P, Kazamias S, López-Martens R, Mauritsson J, Schafer K and Balcou P 2005 *J. Mod. Opt.* **52** 379